Numerical modelling of fluid-induced soil erosion in granular filters using a coupled bonded particle lattice Boltzmann method

Min Wang*, Y.T. Feng, G.N. Pande

Zienkiewicz Centre for Computational Engineering, College of Engineering, Swansea University, SA1 8EP, UK

* Corresponding email: sacewangmin@gmail.com

A.H.C. Chan

School of Engineering and ICT, University of Tasmania, Hobart 7001, Australia

W.X. Zuo

School of Civil Engineering, University of Birmingham, B15 2TT, UK

Abstract

This paper presents a three-dimensional coupled bonded particle and lattice Boltzmann method (BPLBM) with an immersed moving boundary scheme for the fluid-solid interaction. It is then applied to investigate the erosion process of soil particles in granular filters placed within earth dams. The microscopic migration of soil particles can be clearly visualised as the movement of particles can be directly recorded. Three granular filters with different representative size ratios are simulated and the numerical results are seen to match the empirical criteria. In addition, the effect of the representative size ratio of granular filters, hydraulic loading and erosion time are discussed.

Keywords

Internal erosion; Bonded particle method; Lattice Boltzmann method; Granular filter; Immersed moving boundary; Fluid-solid coupling

1. Introduction

Internal erosion of soil particles induced by the hydraulic forces in a dam and its foundations is one of the most common causes of failure of levees, slopes and earth dams. The onset of soil erosion remains un-noticed within an earth structure until it has progressed enough to be

detected during periodic field inspections. Providing a granular filter at an appropriate location is one of the effective ways to eliminate this risk of seepage induced erosion occurring in dams and embankments. It has been adopted in engineering practice for hundred years. However, the performance of granular filters is still not well understood and the designing of granular filters are mainly made according to the empirical criteria derived from experiments.

There has been much progress in the field of physical modelling of the transport of fines in granular filters (Terzaghi and Peck, 1948, Wan and Fell, 2004, Bendahmane et al., 2008, Xiao and Shwiyhat, 2012, Okeke and Wang, 2016). It should be acknowledged the physical experiment is the principal method even now in this research field. The widespread filter design criteria are based on the statistical correlations of experimental observations (Terzaghi and Peck, 1948). These criteria are empirical and constantly revised as long as new experimental data becomes available (Fell et al., 2005, Indraratna et al., 2007, Das and Sobhan, 2013). Due to the complexity of soil erosion, emerging at the microscopic pore/grain level, the experimental methods have limitations in understanding such a complicated issue from the macroscopic viewpoint.

To overcome the problems aforementioned, a few numerical techniques were proposed or applied to the investigation of internal erosion from time to time. Zou et al. (2013) first applied the coupled discrete element method and computational fluid dynamics (DEMCFD) (Tsuji et al., 1993, Xu and Yu, 1997, Wu and Guo, 2012) technique to simulate the transient transport of eroded base-soil particles into a filter. The distributions of the eroded base-soil particles in different filters were traced and analysed. It was found that the eroded mass and intruding depth of the base-soil particles into the filter are related to the representative particle size ratio of the base soil to the filter, hydraulic gradient and erosion time. Then, the migration mechanism of the base soil through granular filters was studied by the same method (Huang et al., 2014). The total eroded base soil mass, the distribution of the eroded particles within the filter and the porosity were observed.

Cui et al. (2014) introduced a two-dimensional coupled discrete element method and lattice Boltzmann method (DEMLBM) (Feng et al., 2007, Cook et al., 2004) to the study of soil erosion induced by local leakage from a buried pipe. The influence factors including flow rates and initial bed heights were considered, and the excess pore pressure distribution and the soil transport due to a localised leak were compared with existing experimental findings.

This coupled two-dimensional technique was also applied to particle detachment and transport in piping erosion (Sibille et al., 2015). Numerical experiments showed that the erosion rate is linearly related to the hydraulic shear stress and the erosion threshold depends on the cohesion of the granular assembly.

Although the DEMLBM has been proven to be promising for internal erosion issues, two potential problems lie in the two-dimensional simulation of fluid-particle systems. First, it is hard to obtain the realistic flow channels in two-dimensional modelling, because the flow paths of fluid are always blocked up by contacted spheres. Attempts to resolve this problem can be seen in the reference (Boutt et al., 2007). The other is that the cohesive force in geomaterials may be considered by the Johnson-Kendall-Roberts (JKR) model (Johnson et al., 1971) or Derjaguin-Muller-Toporov (DMT) model (Derjaguin et al., 1975) in discrete element method (DEM). It should be noticed that these adhesion models are mainly proposed to account for the influence of adhesion, like Van der Waals forces, between fine particles with very small size and low stiffness. To deal with the cohesion forces in a general way in DEMLBM, a two-dimensional bonded particle and lattice Boltzmann method (BPLBM) was proposed (Wang et al., 2016a, Wang et al., 2016b) and its feasibility was well demonstrated.

The main objective of this study is to develop a three-dimensional bonded particle and lattice Boltzmann method and use it to investigate the internal erosion process of soil particles in granular filters. This coupled method can directly deal with the fluid-particle interaction using an immersed moving boundary (IMB) method. Furthermore, the three-dimensional modelling of the migration of soil particles within the skeleton of granular filters by BPLBM gives insights into the microscopic erosion process. For the sake of consistency, a brief description of the coupled BPLBM is given in section 2. However, for further details of theory and computational aspects, readers should refer to Wang et al., 2016a and Wang et al., 2016b. In Section 3, a numerical example of transport of finer particles into a layer of coarser filter is presented. Influence of various parameters such as hydraulic gradient and the representative size ratio are presented. Section 4 gives conclusions and recommendations for future work.

2. Computational Methodology

2.1 Bonded particle method

The bonded particle method (BPM), an extension of DEM, is a combination of discrete element method and lattice method (Schlangen and Garboczi, 1997). In BPM, the treatment of interactions between particles is similar to that in the discrete element method (Cundall and Strack, 1978, Cundall and Strack, 1979) in which particle-particle interactions are treated as a transient problem where an equilibrium state is reached when the internal forces are balanced. Newton's second law is utilised to determine the translation and rotation of each particle arising from the contact forces, e.g., externally applied forces and body forces as well as cohesive forces, whilst the force-displacement law is used to update the contact forces that keep changing due to the relative motion of particles at each contact.

The Newton's second law governing the motion of a particle is given by

$$ma + cv = F_c + F_f + mg \tag{1}$$

$$I\ddot{\theta} = T_c + T_f \tag{2}$$

where m and I are respectively the mass and the moment of inertia of particles, c is a damping coefficient, a and $\ddot{\theta}$ are acceleration and angular acceleration, F_c and T_c are, respectively, contact forces and corresponding torques, F_f and T_f are hydrodynamic forces and corresponding torques. It should be emphasized that F_c can be either particle-particle contact forces for granular particles or cohesion forces F_b existing between bonded particles.

2.1.1 The particle-particle contact model

The particle-particle contact force F_c has two components, the normal contact force and the tangential contact force, and they are, respectively, given by

Normal interaction laws:

$$F_n = K_n \delta^m \tag{3}$$

Coulomb friction model:

$$F_t = -\frac{\dot{\delta}_t}{\left|\dot{\delta}_t\right|} \begin{cases} K_t\left|\delta_t\right|; & \left|K_t\delta_t\right| \le \mu F_n \\ \mu F_n; & \left|K_t\delta_t\right| > \mu F_n \end{cases} \tag{4}$$

where K_n and K_t are normal stiffness and tangential stiffness, δ_t and $\dot{\delta}_t$ correspond to accumulated tangential sliding and sliding velocity, δ is the overlap of two particles. The coefficient m can be 1 and 3/2, the former is for the linear contact and the latter is for the Hertz contact model (Oda and Iwashita, 1999). The normal stiffness in Hertz contact model is defined as

$$K_n = \frac{4E^* \sqrt{R^*}}{3} \tag{5}$$

$$\frac{1}{\mathrm{R}^*} = \frac{1}{\mathrm{R}_{[\mathrm{A}]}} + \frac{1}{\mathrm{R}_{[\mathrm{B}]}}, \qquad \frac{1}{\mathrm{E}^*} = \frac{1\text{-}\upsilon_{[\mathrm{A}]}^2}{\mathrm{E}_{[\mathrm{A}]}} + \frac{1\text{-}\upsilon_{[\mathrm{B}]}^2}{\mathrm{E}_{\mathrm{B}}} \tag{6}$$

where $\upsilon_{[A]}, \upsilon_{[B]}$ are, respectively the Poisson's ratios of particle A and B. $R_{[A]}$, $E_{[A]}$, $R_{[B]}$ and $E_{[B]}$ are the radii and Young's moduli of particle A and B.

An alternative of the Coulomb friction model is the commonly used Mindlin-Deresiewicz model (Thornton and Yin, 1991, Oda and Iwashita, 1999, Vu-Quoc et al., 2004). In this model, the tangential force is dependent on both loading history and the magnitude of the normal force.

2.1.2 Bond models

The initial bond model proposed is referred to as the 'contact bond model' (Itasca Consulting Group Inc, 2002, Potyondy and Cundall, 2004). It approximates the physical behaviour of a vanishingly small cemented-like substance joining the two bonded particles. It can be envisioned as a pair of elastic springs (or a point of glue) with constant and shear stiffness acting at the contact point. These two springs have specified shear and tensile strengths. The existence of a contact bond precludes the possibility of slip.

2.1.2.1 Contact bond model

The two components of the contact bond model can be described as follows:

Normal component:

$$F_n^b = \begin{cases} \mathrm{K}_n^b \delta; & F_n^b \le F_{bn} \\ 0; & F_n^b > F_{bn} \end{cases} \tag{7}$$

Tangential component:

$$F_t^b = \begin{cases} \mathrm{K}_t^b |\delta_t|; & F_t^b \le F_{bt} \\ 0; & F_t^b > F_{bt} \end{cases} \tag{8}$$

where K_n^b and K_t^b are the normal stiffness and tangential stiffness for the cement, F_{bn} is the critical tensile force and F_{bt} is the critical shear strength.

When the tensile contact force equals or exceeds the normal contact bond strength, the bond breaks. Both normal and shear bond forces are set to be zero. In contrast to this, when the shear contact force is equal or greater than the shear contact bond strength, the bond breaks, but only tangential bond force becomes zero.

2.1.2.2 Advanced bond model

This widely accepted contact bond model accounts for forces acting at the contact point, but it is unable to describe the real history-dependent friction behaviour of the bond. It has been reported that more advanced bond models can reproduce more complicated mechanical behaviours (Delenne et al., 2004, Jiang et al., 2012).

An advanced contact bond model which includes a normal bond considering softening effect and a history dependent Coulomb friction model was proposed recently (Wang, 2016), and this proposed bond model is used in this research. It is found that this advanced normal bond model delineated in Figure 1 can capture the macroscopic softening process and alleviate the problem emerging in spring bond models.

Normal component:

$$F_n^b = \begin{cases} K_n^b \delta & \delta >= \delta_1 \\ K_n^b \delta_1 + K_{sf}(\delta - \delta_1) & \delta_2 < \delta < \delta_1 \\ 0 & \delta < \delta_2 \end{cases} \tag{9}$$

Tangential component:

$$F_t^b = -\frac{\dot{\delta}_t}{\left|\dot{\delta}_t\right|} \begin{cases} K_t^b \left|\delta_t\right|; & \left|K_t^b \delta_t\right| \le \mu F_n^b \\ \mu F_n^b; & \left|K_t^b \delta_t\right| > \mu F_n^b \end{cases} \tag{10}$$

where K_{sf} , δ_1 and δ_2 are the stiffness for softening period, overlap corresponding to critical bond strength and overlap corresponding to bond breakage, respectively.

2.2 Lattice Boltzmann method

The lattice Boltzmann method (LBM) (Chen et al., 1991) emerged as an alternative of traditional computational fluid dynamics (CFD). It has been attracting more and more researchers' interest. The primary variables of LBM are fluid density distribution functions

instead of pressure and velocity considered in the conventional CFD. In LBM, the fluid domain is divided into regular lattices and the fluid is simplified as a group of mesoscopic particle packages rest at lattice nodes. Each particle package includes several fluid particles which are allowed to move to the adjacent lattice nodes or stay at rest. During each discrete time step, fluid particles at individual lattice nodes move to their immediate neighbouring lattice nodes along the given directions. Thus, at each node, collision occurs between the fluid particles from the neighbouring nodes. The macro fluid behaviour can be described through the statistics of the motion of fluid particles. Unlike the traditional CFD methods, which solve the conservation (Navier-Stokes) equations of macroscopic properties (i.e., mass, momentum, and energy) numerically, LBM models the fluid flow though resolving the propagation and collision processes of fluid particles, which are governed by the lattice Boltzmann equation. In particular, the Navier-Stokes equations can be recovered from the lattice Boltzmann equation under the condition of low Mach numbers (Chen et al., 1992).

2.2.1 Bhatnagar-Gross-Krook (BGK) model

Due to the high computational efficiency and ease in programming, the widely used BGK model is adopted in this work. It can be characterised by the following lattice Boltzmann equation:

$$f_i(\boldsymbol{x} + \boldsymbol{e}_i \Delta t, t + \Delta t) - f_i(\boldsymbol{x}, t) = \Omega \tag{11}$$

where f_i is the primary variables (so-called fluid density distribution functions), and Ω is the collision operator. In the BGK Model, Ω is characterised by a relaxation time τ and the equilibrium distribution function $f_i^{eq}(x, t)$.

$$\Omega = -\frac{\Delta t}{\tau}\left[f_i(\boldsymbol{x}, t) - f_i^{eq}(\boldsymbol{x}, t)\right] \tag{12}$$

The D3Q15 model is the most popular 3D one and it uses a cubic lattice with 15 discrete velocity directions. The fluid particles at each lattice node move to their 14 neighbouring nodes with discrete velocities $\boldsymbol{e_i}$, (i =1-14). A proportion of the particles, with velocity $\boldsymbol{e_0}$, remain at the node. With reference to the numbering system in Figure 2, the 15 discrete velocity vectors correspond to the column vectors of the following matrix in lattice unit:

$$E = \begin{bmatrix} 0 & 1 & -1 & 0 & 0 & 0 & 0 & 1 & -1 & 1 & -1 & 1 & -1 & 1 & -1 \\ 0 & 0 & 0 & 1 & -1 & 0 & 0 & 1 & -1 & 1 & -1 & -1 & 1 & -1 & 1 \\ 0 & 0 & 0 & 0 & 0 & 1 & -1 & 1 & -1 & -1 & 1 & 1 & -1 & -1 & 1 \end{bmatrix}$$

The corresponding equilibrium distribution function can be defined as

$$f_i^{eq} = \omega_i \rho (1 + \frac{3}{C^2} \boldsymbol{e_i} \cdot \boldsymbol{v} + \frac{9}{2C^4} (\boldsymbol{e_i} \cdot \boldsymbol{v})^2 - \frac{3}{2C^2} \boldsymbol{v} \cdot \boldsymbol{v}) \qquad (i = 0,...,15) \tag{13}$$

Its weighting factors are defined as:

$$\omega_0 = \frac{2}{9}, \qquad \omega_{1\text{-}6} = \frac{1}{9}, \qquad \omega_{7\text{-}14} = \frac{1}{72} \tag{14}$$

In LBM, the macroscopic fluid density and velocity can be calculated from the distribution functions

$$\rho = \sum_{i=0}^{14} f_i, \qquad \rho \boldsymbol{v} = \sum_{i=1}^{14} f_i \boldsymbol{e_i} \tag{15}$$

The fluid pressure is given by

$$P = C_S^2 \rho \tag{16}$$

where C_S is termed the fluid speed of sound and is related to the lattice speed C

$$C_S = C / \sqrt{3} \tag{17}$$

The relaxation parameter, τ, used in our program is implicitly determined by

$$\tau = \frac{3\upsilon \Delta t}{h^2} + \frac{1}{2} == \frac{3\upsilon}{Ch} + \frac{1}{2} \tag{18}$$

The kinematic viscosity, υ, of the fluid under consideration is constant during the whole simulation.

2.2.2 Body force

Many efforts have been made to consider the body force in the framework of LBM in past twenty years (He et al., 1997, Buick and Greated, 2000, Guo et al., 2002, Mohamad and Kuzmin, 2010, Silva and Semiao, 2011). In this work the extensively used Guo's method (Guo et al., 2002) is adopted.

The body force density **F** (for gravity $F = \rho g$) was first considered by modifying the equilibrium density distribution functions.

$$f_i^{eq} = \omega_i \rho (1 + \frac{3}{C^2} e_i \cdot v^* + \frac{9}{2C^4} (e_i \cdot v^*)^2 - \frac{3}{2C^2} v^* \cdot v^*) \quad (i = 0,...,14) \tag{19}$$

where v^* is the equilibrium velocity which is given by

$$\rho u = \rho v^* = \rho v + 0.5F \tag{20}$$

Then, an additional term was added to the collision operator

$$\Omega = -\frac{\Delta t}{\tau} [f_i(x, t) - f_i^{eq}(x, t)] + \Delta t F_i \tag{21}$$

where F_i is defined as

$$F_i = \omega_i (1 - \frac{1}{2\tau}) \left[\frac{e_i - u}{C_S^2} + \frac{e_i (e_i \cdot u)}{C_S^4} \right] \cdot F \tag{22}$$

2.3 The fluid-solid coupling

Much work on the fluid-solid coupling schemes in the framework of LBM has been made (Ladd, 1994, Noble and Torczynski, 1998, Lallemand and Luo, 2003, Wu and Shu, 2009). Amongst them, the immersed moving boundary method receives the most attention in the coupled DEMLBM technique due to its good stability and accuracy.

2.3.1 Immersed moving boundary method

The immersed moving boundary scheme was proposed by Noble and Torczynski (1998) to overcome fluctuations of hydrodynamic forces calculated by the modified bounce back technique. In this method, the solid particle is represented by solid nodes, the solid boundary nodes and interior solid nodes. The fluid nodes near solid boundary nodes are defined as fluid boundary nodes. To facilitate the illustration of the 3D IMB scheme, a cross-section through the centre of a sphere is given in Figure 3. Four sorts of nodes, solid boundary nodes, interior solid nodes, fluid boundary nodes and normal fluid nodes, are, respectively, marked in red, yellow, green and blue. In order to retain the advantages of LBM, namely the locality of the collision operator and the simple linear streaming operator, an additional collision term, Ω_i^s, for nodes covered partially or fully by the solid is introduced to the standard collision

operator of LBM. The modified collision operator for resolving the fluid-solid interaction is given by

$$\Omega = -\frac{\Delta t}{\tau}(1-B)[f_i(\boldsymbol{x},t) - f_i^{eq}(\boldsymbol{x},t)] + (1-B)\Delta t F_i + B\Omega_i^S \tag{23}$$

where B is a weighting function that depends on the local solid ratio ε, defined as the fraction of the nodal volume; F_i is the body force term.

$$B = \frac{\varepsilon(\tau - 0.5)}{(1-\varepsilon) + (\tau - 0.5)} \tag{24}$$

$$\varepsilon = V_S / V_N \tag{25}$$

V_S is the nodal volume occupied by the solid particle and V_N is the whole nodal volume.

The additional collision term is based on the bounce-rule for non-equilibrium part of the particle distribution and is given by

$$\Omega_i^S = f_{-i}(\boldsymbol{x},t) - f_i(\boldsymbol{x},t) + f_i^{eq}(\rho, U_S) - f_{-i}^{eq}(\rho, u) \tag{26}$$

where U_S is the velocity of the solid node and u is the velocity of the fluid part at the node.

The velocity of the solid node considering the effect of particle rotation is described by

$$U_S = U_P + \omega \times \mathrm{l_P} \qquad (\mathrm{l_P} = \sqrt{(\mathrm{x}-\mathrm{x_P})^2 + (\mathrm{y}-\mathrm{y_P})^2 + (\mathrm{z}-\mathrm{z_P})^2}) \tag{27}$$

U_P and ω are the velocity and angular velocity of the solid particle.

The resultant hydrodynamic force in Eq. 1 and torque in Eq. 2 exerted on the solid can be calculated by

$$F_f = Ch\Big[\sum_n (B_n \sum_i \Omega_i^s e_i)\Big] \tag{28}$$

$$T_f = Ch\Big\{\sum_n \big[(\boldsymbol{x} - \boldsymbol{x}_P) \times (B_n \sum_i \Omega_i^s e_i)\big]\Big\} \tag{29}$$

3. Numerical Tests

3.1 Empirical criteria for granular filter design

In engineering practice, the grain-size distribution of the filter should be properly managed to avoid the danger of erosion or piping. The aim is to allow fluid (water) to pass through the

soil medium without erosion of the protected base material, and if some material does pass through, it should not clog the filter. Generally speaking, two conditions should be satisfied:

a) The size of the voids in the filter material should be small enough to hold the larger particles of the protected material in place.
b) The filter material should have a high hydraulic conductivity to prevent build-up of large seepage forces and hydrostatic pressures in the filters.

To be specific, the effective diameter of the pore spaces in the filter should be less than D_{85} of the soil to be protected and the effective pore diameter is about 0.2 D_{15} to 0.25D_{15} of the filter. Based on this idea, Terzaghi and Peck (1948) proposed the following design criteria (Zou et al., 2013, Huang et al., 2014):

$$R_1 = \frac{D_{15(F)}}{D_{85(S)}} \leq 4 \quad \text{(to satisfy condition a)} \tag{30}$$

$$R_2 = \frac{D_{15(F)}}{D_{15(S)}} \geq 5 \quad \text{(to satisfy condition b)} \tag{31}$$

where $D_{15(F)}$ - diameter through which 15% of filter material will pass;

$D_{15(S)}$ - diameter through which 15% of soil to be protected will pass;

$D_{85(S)}$ - diameter through which 85% of soil to be protected will pass.

3.2 Numerical model

Here, we solve a simple one dimensional problem where it would be possible to verify the complex three dimensional problem. A base soil-filter system (Figure 4 in lattice unit) is modelled by a cubic sample (0.1 m×0.1 m×0.2 m). The lateral boundaries are fixed walls. A stationary wall, only effective for solid particles, is used to support the base soils and the granular filter, whilst the upper surface of the granular filter is fixed. The simulations in this section are carried out using our in-house program (BPLBM3D) on the personal computer (Intel Core i5-3450 CPU@3.10GHz).

The base soil, so-called the protected soil, is comprised of 1500 various-sized spherical particles. In engineering practice, the slightly cohesive force exists between natural sands. In this work, the cohesion is considered through the aforementioned advanced bond model in BPM. In order to demonstrate the feasibility and accuracy of the proposed method, three filters, with different size ratios R_1=2.29, 3.43 and 4.29, are constructed. Two of them comply

with the empirical criterion (Equations 30 and 31) and one filter disobeys it. During the whole simulation, a constant hydraulic pressure is applied at the bottom. The lattice space adopted is 1.0 mm, thus the problem domain is divided into 100×200 grids. The time step used is 1.667×10^{-5} s. Specific parameters for the numerical model are given in Table 1. The particle size distribution curves of the protected soil and filters are shown in Figure 5.

In addition, to investigate the effect of hydraulic gradient on the migration of soil particles in granular filters, simulations with different hydraulic loads are carried out on the soil-filter system with R_1=4.29.

3.3 Results and discussions

a) Migration process of fine particles in filters

In this paper, the base soil and granular filter are represented in colours regarding to their particle sizes. Figure 6 shows snapshots of the performance of the coarse filter (R_1=4.29) at different time instants. It can be found that the particles of the base soils gradually intrude into the granular filter under the hydraulic loading at t = 0.6668 s. With the progress of simulation, some fine and coarse particles of the protected soil start to penetrate the coarse filter. Finally, considerable base soils, almost 10%, are washed away at the end of simulation (t=1.667 s).

Figure 7 gives the distribution curves of the number of soil particles versus the vertical location at different time instants. Therefore, the migration of soil particles at each stage in the filter can be recorded. We find that with the progress of simulation soil particles will invade to further depth, and more soil particles can be washed out of the filter.

b) Comparison of filters with different size ratios

To examine the effect of the size ratio on the performance of granular filters, three filters with different size ratios are simulated and compared with regard to the migration of base soils in filters and soil erosion ratios. During the whole simulation of the performance of granular filters, the transport of base soils and the evolution of hydraulic pressures can be successfully investigated. To observe the distribution of soil particles in the filter more clearly, the snapshots for three models at the end of simulations are given in Figure 8. It can be found that both fine and coarse particles of the protected soil pass through the coarse filter with R_1=4.29. While, only part of fine particles can pass through the intermediate filter with

R_1=3.43 and few soil particles are eroded in the fine filter R_1=2.29. Thus the intermediate and fine filters, which comply with the empirical criteria, can effectively alleviate or eliminate the appearance of particle erosions.

In order to better understand the progress of soil erosion process, a quantitative ratio is introduced and it is defined as the percentage of the mass of eroded particles over the total mass of the base soil (see Equation 32). The soil particles whose vertical position exceeds a certain distance Z, e.g. 0.17 m in this model, from the bottom are treated as eroded particles.

$$R_{erosion} = \frac{Mass_{erosion}}{Mass_{soil}} = \frac{\sum_{i=1}^{N_l} r_i}{\sum_{i=1}^{N} r_i} \tag{32}$$

where N_l and N are respectively the numbers of eroded particles and the total number of the base soil, r_i is the radius of the particle under consideration.

Figure 9 gives the final distribution curves (at t= 1.667 s) of the number of eroded particles versus the invasion depth. These curves show that with the increase of size ratios more soil particles can be washed away to a height over 0.17 m. Based on other related parameters, such as radius and number, of eroded particles, the corresponding erosion ratio can be computed using Equation 32.

From Figure 10, it can be observed at the earlier stage of simulations soil particles transport at a low speed and no eroded particles can be detected. A certain time later, the erosion ratio of protected soils increases rapidly. The final erosion ratios are 10.0% for the coarse filter, 0.5% for the intermediate filter and 0.0% for the fine filter, respectively.

c) Effect of hydraulic gradient on erosion

To investigate the effect of hydraulic gradient on soil erosion, five hydraulic loadings, i.e. 17361.11 Pa, 15625.0 Pa, 13020.83 Pa, 11284.72 Pa and 8680.56 Pa, are applied to the bottom boundary of the filter with size ratio R_1=4.29. The corresponding hydraulic gradient can be calculated using the following equation

$$\boldsymbol{i} = \frac{P}{\rho g H} \tag{33}$$

where P is the applied pressure difference; ρ and H are respectively the fluid density and the vertical height of the model.

Figure 11 shows the final distribution of soil particles under different gradients. The variation of eroded particles undergoing different hydraulic gradients are traced and compared in Figure 12, and the relationship of the erosion ratio of base soil and the elapsed time are shown in Figure 13. It can be found that with the increase of hydraulic loading more particles can pass through this filter, which leads to a higher erosion ratio. When hydraulic gradient is 4.43, the number of eroded particles is 47. The eroded particles increase to 146 when the hydraulic gradient increases to 8.86.

The coupled BPLBM technique has been well demonstrated from the above numerical tests. The BPM successfully simulates the natural sand with cohesion and the microscopic transport of particles in the granular filter; whist the LBM and IMB coupling scheme can better resolve the pore fluid flow and fluid-particle interactions at the grain level. Compared to the existing continuum methods, the BPLBM could capture the fluid flow and fluid-solid interactions at the microscopic scale. In addition, this coupled technique could directly approach the fluid-particle interaction without introducing the averaging technique for the fluid-particle interactions in DEMCFD. It is demonstrated that the coupled BPLBM can investigate the particle erosion issue in granular filter from a different point of view. The microscopic particle transportation and pore fluid flow further an engineer's understanding of such complex fluid-particle systems.

The three-dimensional simulation in this research is a carried out using a personal computer (Intel Core i5-3450 CPU@3.10GHz). For each simulation, it takes about 48 hours 57 minutes. The application to larger-sized problem seems to be impossible at the present stage. Therefore, parallelization of the proposed technique will be our next work in the near future.

4. Conclusions

In this paper, a three-dimensional bonded particle and lattice Boltzmann method is introduced and used to investigate the internal erosion process of soil particles in granular filters. Different to the treatment in DEMCFD where the empirical equations are required for the computing of drag forces, the fluid-solid coupling is achieved by directly solving the collision between the fluid particles and solid nodes in the framework of lattice Boltzmann method.

Three granular filters with different size ratios are simulated and the numerical results are compared with the empirical design criteria. The microscopic migration of soil particles within granular filters can be readily observed through BPLBM and the eroded particles can be traced. It is found that with the increase of representative size ratio R1 of granular filters the erosion percentage of soil particles gradually grows. When the size ratio R1 is increased to a value greater than 4.0 which is the critical value obtained by the empirical criteria, coarse particles of the protected soil will pass through the filter. These results match the empirical design criteria very well. In addition, more particles can penetrate a granular filter under a higher hydraulic loading, which leads to a higher erosion ratio. Therefore, it is well demonstrated the coupled BPLBM approach gains a deeper insight into the internal erosion process in dams.

It should be mentioned that only spheres are used to simulate soil particles at the initial stage. Non-spherical particles are supposed to be more fruitful. The implementation of irregular particles into BPLBM will be carried out in the following stage.

Acknowledgements

The research work was supported by the National Natural Science Foundation of China (Grant No. 51579237) and the Foundation of State Key Laboratory for Geomechanics and Deep Underground Engineering (Grant No. SKLGDUEK 1110). The authors are very grateful to their financial support. The authors also would like to thank the editor and two anonymous reviewers for their constructive comments, which helped us to improve the manuscript.

References

Bendahmane, F., Marot, D. & Alexis, A. 2008. Experimental Parametric Study of Suffusion and Backward Erosion. *Journal of Geotechnical and Geoenvironmental Engineering,* 134**,** 57-67.

Boutt, D. F., Cook, B. K., Mcpherson, B. J. O. L. & Williams, J. R. 2007. Direct simulation of fluid-solid mechanics in porous media using the discrete element and lattice-Boltzmann methods. *Journal of Geophysical Research* 112, B10209.

Buick, J. M. & Greated, C. A. 2000. Gravity in a lattice Boltzmann model. *Physical Review E,* 61, 5307-5320.

Chen, H., Chen, S. & Matthaeus, W. H. 1992. Recovery of the Navier-Stokes equations using a lattice-gas Boltzmann method. *Phys, Rev. A*, 45**,** 5339-5342.

Chen, S., Chen, H., Martinez, D. O. & W. H. Matthaeus 1991. Lattice Boltzmann model for simulation of magnetohydrodynamics. *Phys. Rev. Lett.,* 67**,** 3776-3779.

Cook, B. K., Noble, D. R. & Williams, J. R. 2004. A direct simulation method for particle-fluid systems. *Engineering Computations,* 21**,** 151-168.

Cui, X., Li, J., Chan, A. & Chapman, D. 2014. Coupled DEM–LBM simulation of internal fluidisation induced by a leaking pipe. *Powder Technology,* 254**,** 299-306.

Cundall, P. A. & Strack, O. D. L. 1978. The distinct element method as a tool for research in granular media. *Report to the National Science Foundation Concerning NSF Grant ENG76-20711*.

Cundall, P. A. & Strack, O. D. L. 1979. A discrete numerical model for granular assemblies. *Geotechnique,* 29**,** 47-65.

Das, B. & Sobhan, K. 2013. *Principles of geotechnical engineering[M]*, Cengage Learning.

Delenne, J.-Y., El Youssoufi, M. S., Cherblanc, F. & Bénet, J.-C. 2004. Mechanical behaviour and failure of cohesive granular materials. *International Journal for Numerical and Analytical Methods in Geomechanics,* 28**,** 1577-1594.

Derjaguin, B. V., Muller, V. M. & Toporov, Y. P. 1975. Effect of contact deformations on the adhesion of particles. *Journal of Colloid and Interface Science,* 53**,** 314-326.

Fell, R., Macgregor, P., Stapledon, D. & Bell, G. 2005. *Geotechnical engineering of dams*, CRC Press.

Feng, Y. T., Han, K. & Owen, D. R. J. 2007. Coupled lattice Boltzmann method and discrete element modelling of particle transport in turbulent fluid flows: Computational issues. *International Journal for Numerical Methods in Engineering,* 72**,** 1111-1134.

Guo, Z., Zheng, C. & Shi, B. 2002. Discrete lattice effects on the forcing term in the lattice Boltzmann method. *Physical Review E,* 65**,** 046308.

He, X., Zou, Q., Luo, L.-S. & Dembo, M. 1997. Analytic solutions of simple flows and analysis of nonslip boundary conditions for the lattice Boltzmann BGK model. *Journal of Statistical Physics,* 87, 115-36.

Huang, Q.-F., Zhan, M.-L., Sheng, J.-C., Luo, Y.-L. & Su, B.-Y. 2014. Investigation of fluid flow-induced particle migration in granular filters using a DEM-CFD method. *Journal of Hydrodynamics, Ser. B,* 26**,** 406-415.

Indraratna, B., Raut, A. & Khabbaz, H. 2007. Constriction-Based Retention Criterion for Granular Filter Design. *Journal of Geotechnical and Geoenvironmental Engineering,* 133**,** 266-276.

Itasca Consulting Group Inc 2002. Particle Flow Code in 2 Dimensions. *version 3.0. Minnesota, U.S.A.*

Jiang, M. J., Sun, Y. G., Li, L. Q. & Zhu, H. H. 2012. Contact behavior of idealized granules bonded in two different interparticle distances: An experimental investigation. *Mechanics of Materials,* 55.

Johnson, K. L., Kendall, K. & Roberts, A. D. 1971. Surface Energy and the Contact of Elastic Solids. *Proceedings of the Royal Society of London A: Mathematical, Physical and Engineering Sciences,* 324**,** 301-313.

Ladd, A. J. C. 1994. Numerical simulations of particulate suspensions via a discretized Boltzmann equation. Part 1. Theoretical foundation. *Journal of Fluid Mechanics,* 271**,** 285-309.

Lallemand, P. & Luo, L.-S. 2003. Lattice Boltzmann method for moving boundaries. *Journal of Computational Physics,* 184**,** 406-421.

Mohamad, A. A. & Kuzmin, A. 2010. A critical evaluation of force term in lattice Boltzmann method, natural convection problem. *International Journal of Heat and Mass Transfer,* 53**,** 990-996.

Noble, D. R. & Torczynski, J. R. 1998. A Lattice-Boltzmann Method for Partially Saturated Computational Cells. *International Journal of Modern Physics C,* 09**,** 1189-1201.

Oda, M. & Iwashita, K. 1999. Mechanics of Granular Materials: An Introduction. *A.A. Balkema, Rotterdam*.

Okeke, A. C.-U. & Wang, F. 2016. Hydromechanical constraints on piping failure of landslide dams: an experimental investigation. *Geoenvironmental Disasters,* 3**,** 1-17.

Potyondy, D. O. & Cundall, P. A. 2004. A bonded-particle model for rock. *International Journal of Rock Mechanics and Mining Sciences,* 41**,** 1329-1364.

Schlangen, E. & Garboczi, E. J. 1997. Fracture simulations of concrete using lattice models: Computational aspects. *Engineering Fracture Mechanics,* 57, 319-332.

Sibille, L., Lominé, F., Poullain, P., Sail, Y. & Marot, D. 2015. Internal erosion in granular media: direct numerical simulations and energy interpretation. *Hydrological Processes,* 29**,** 2149-2163.

Silva, G. & Semiao, V. 2011. A study on the inclusion of body forces in the lattice Boltzmann BGK equation to recover steady-state hydrodynamics. *Physica A: Statistical Mechanics and its Applications,* 390, 1085-1095.

Terzaghi, K. & Peck, R. B. 1948. *Soil Mechanics in Engineering Practice*, New York, Wiley.

Thornton, C. & Yin, K. K. 1991. Impact of elastic spheres with and without adhesion. *Powder Technology,* 65**,** 153-166.

Tsuji, Y., Kawaguchi, T. & Tanaka, T. 1993. Discrete particle simulation of two-dimensional fluidized bed. *Powder Technology,* 77**,** 79-87.

Vu-Quoc, L., Lesburg, L. & Zhang, X. 2004. An accurate tangential force–displacement model for granular-flow simulations: Contacting spheres with plastic deformation, force-driven formulation. *Journal of Computational Physics,* 196**,** 298-326.

Wan, C. & Fell, R. 2004. Investigation of Rate of Erosion of Soils in Embankment Dams. *Journal of Geotechnical and Geoenvironmental Engineering,* 130**,** 373-380.

Wang, M. 2016. *A Coupled Bonded Particle and Lattice Boltzmann Method with its Application to Geomechanics.* PhD, Swansea University, UK.

Wang, M., Feng, Y. T. & Wang, C. Y. 2016a. Coupled bonded particle and lattice Boltzmann method for modelling fluid–solid interaction. *International Journal for Numerical and Analytical Methods in Geomechanics,* 40**,** 1383-1401.

Wang, M., Feng, Y. T. & Wang, C. Y. 2016b. Numerical investigation of initiation and propagation of hydraulic fracture using the coupled Bonded Particle–Lattice Boltzmann Method. *Computers & Structures*, in press.

Wu, C.-Y. & Guo, Y. 2012. Numerical modelling of suction filling using DEM/CFD. *Chemical Engineering Science,* 73**,** 231-238.

Wu, J. & Shu, C. 2009. Implicit velocity correction-based immersed boundary-lattice Boltzmann method and its applications. *Journal of Computational Physics,* 228**,** 1963-1979.

Xiao, M. & Shwiyhat, N. 2012. Experimental Investigation of the Effects of Suffusion on Physical and Geomechanic Characteristics of Sandy Soils. *Geotechnical Testing Journal,* 35**,** 1-11.

Xu, B. H. & Yu, A. B. 1997. Numerical simulation of the gas-solid flow in a fluidized bed by combining discrete particle method with computational fluid dynamics. *Chemical Engineering Science,* 52**,** 2785-2809.

Zou, Y.-H., Chen, Q., Chen, X.-Q. & Cui, P. 2013. Discrete numerical modeling of particle transport in granular filters. *Computers and Geotechnics,* 47**,** 48-56.

Table 1

Table 1 Parameters for the filter-soil system

Parameter	Value	Parameter	Value
Particle density /kg/m^3	2750	Fluid density /kg/m^3	1000
Friction coefficient	0.3	kinematic viscosity υ	1.0×10^{-6}
Particle contact stiffness /N/m	5.0×10^7	Bond normal stiffness /N/m	5.0×10^5
Bond strength /N	10	Bond shear stiffness /N/m	1.0×10^5
Contact damping ratio ξ	0.5	Smagorinsky constant S_c	0.1

Figures list

Figure 1a
Click here to download high resolution image

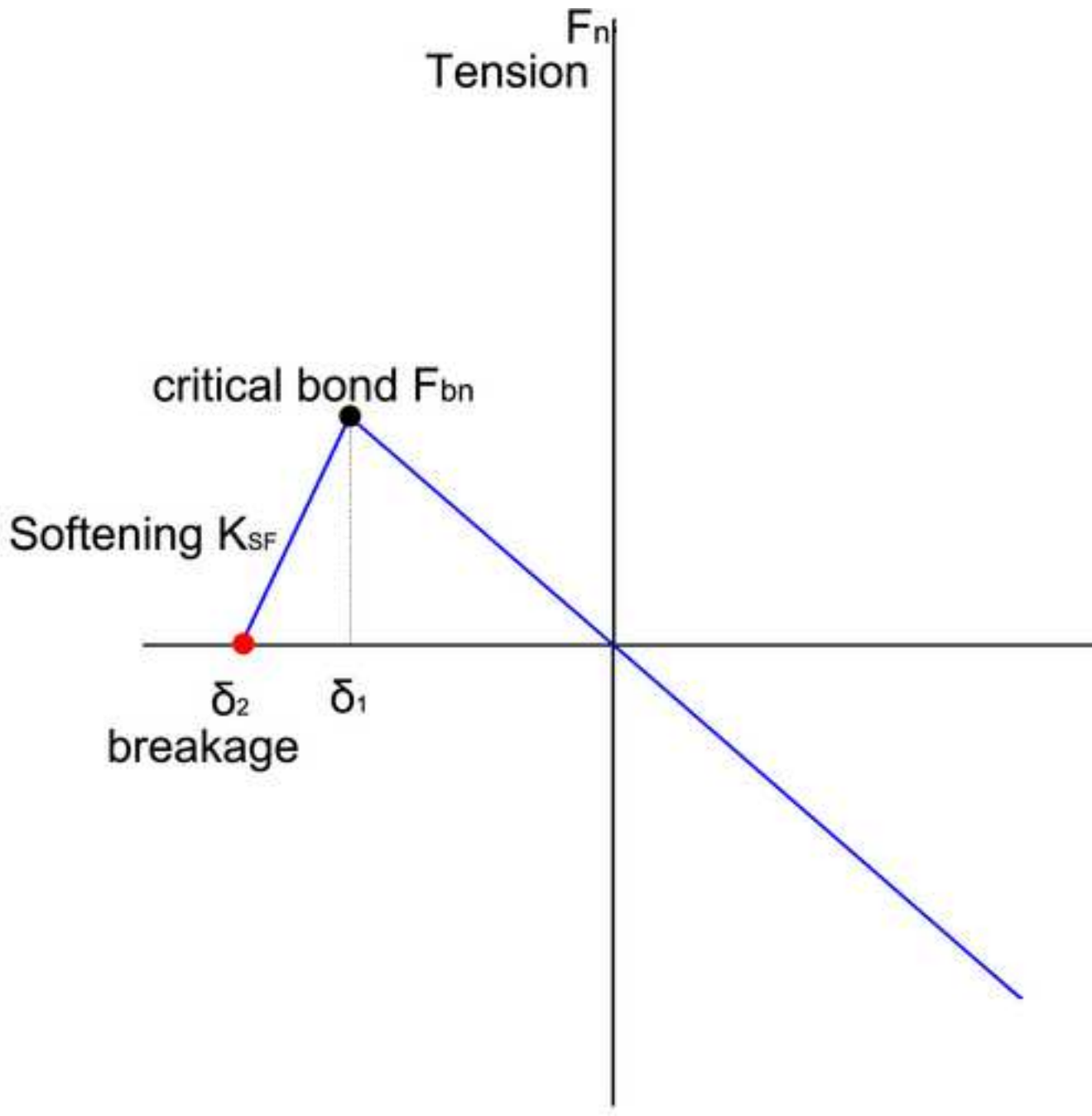

Figure 1b
Click here to download high resolution image

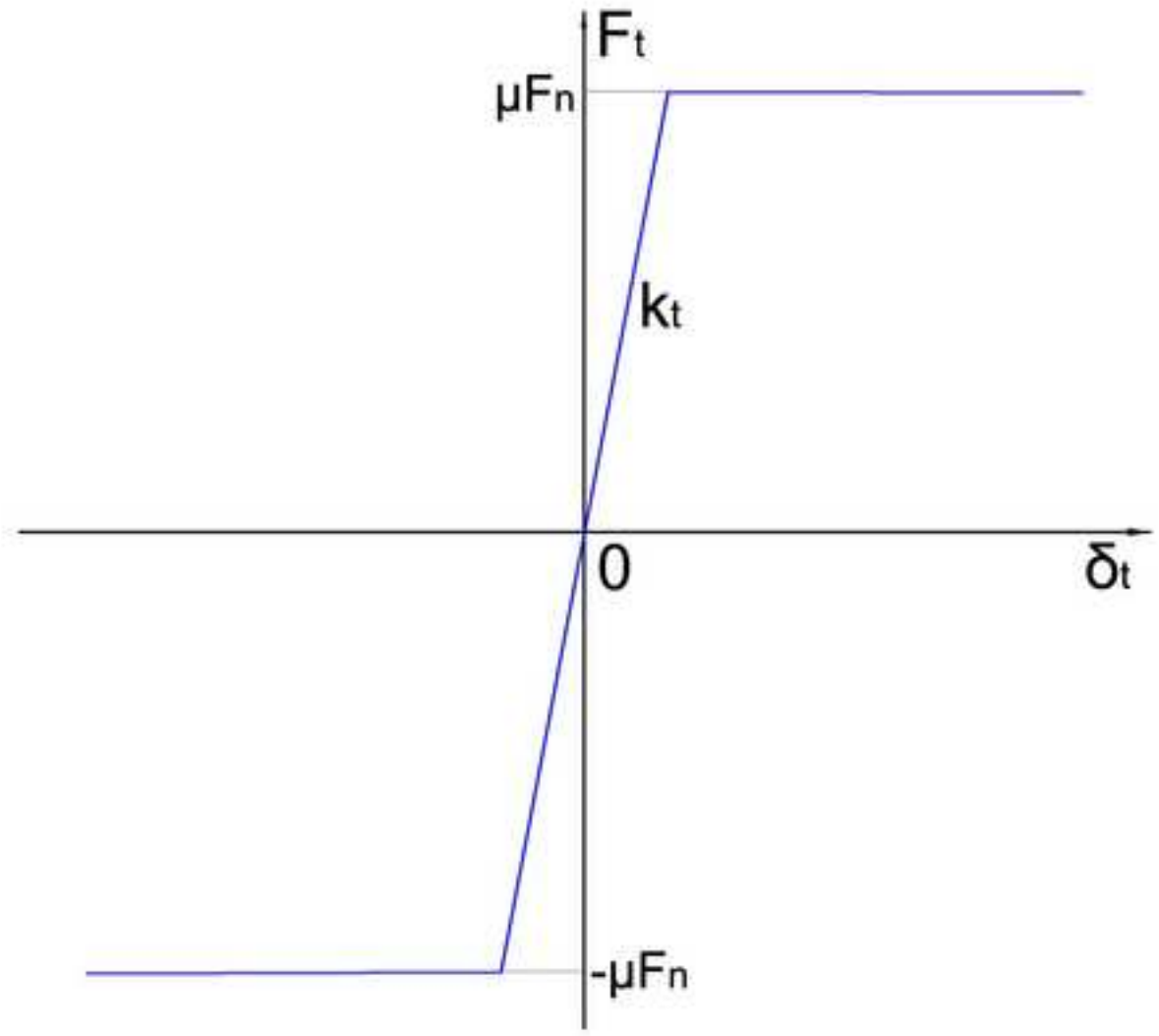

Figure 2
Click here to download high resolution image

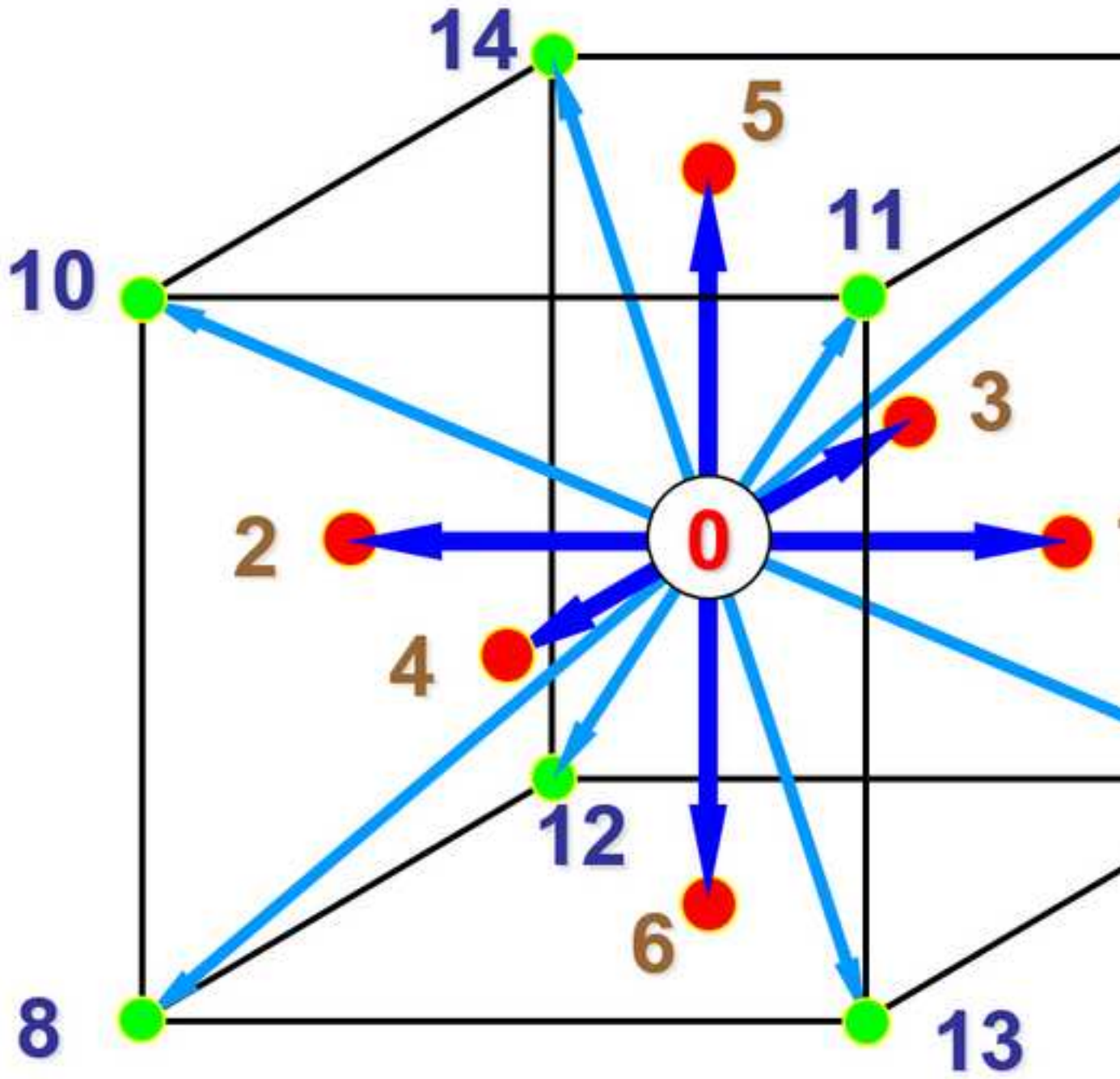

Figure 3
Click here to download high resolution image

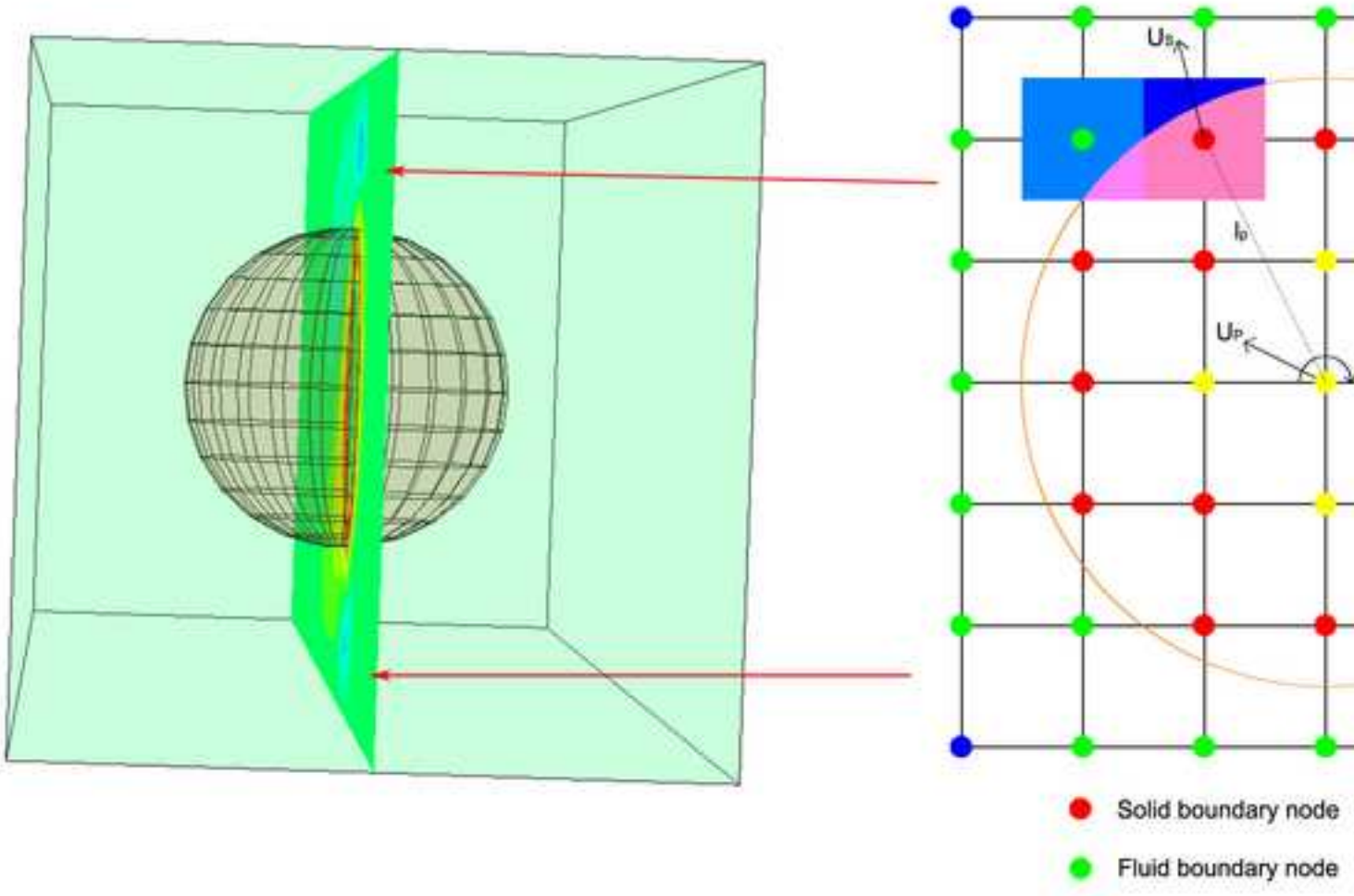

Figure 4
Click here to download high resolution image

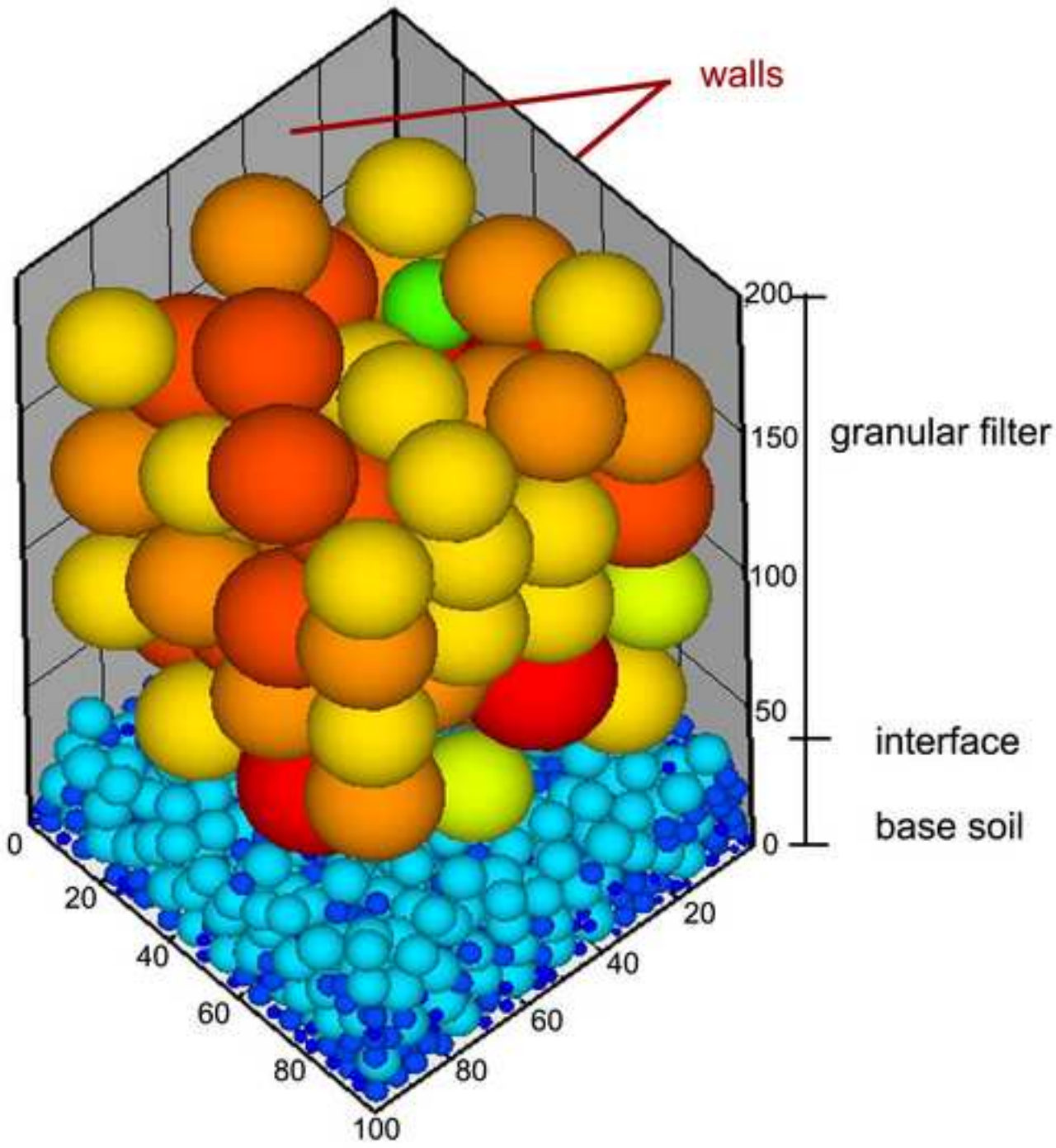

Figure 5

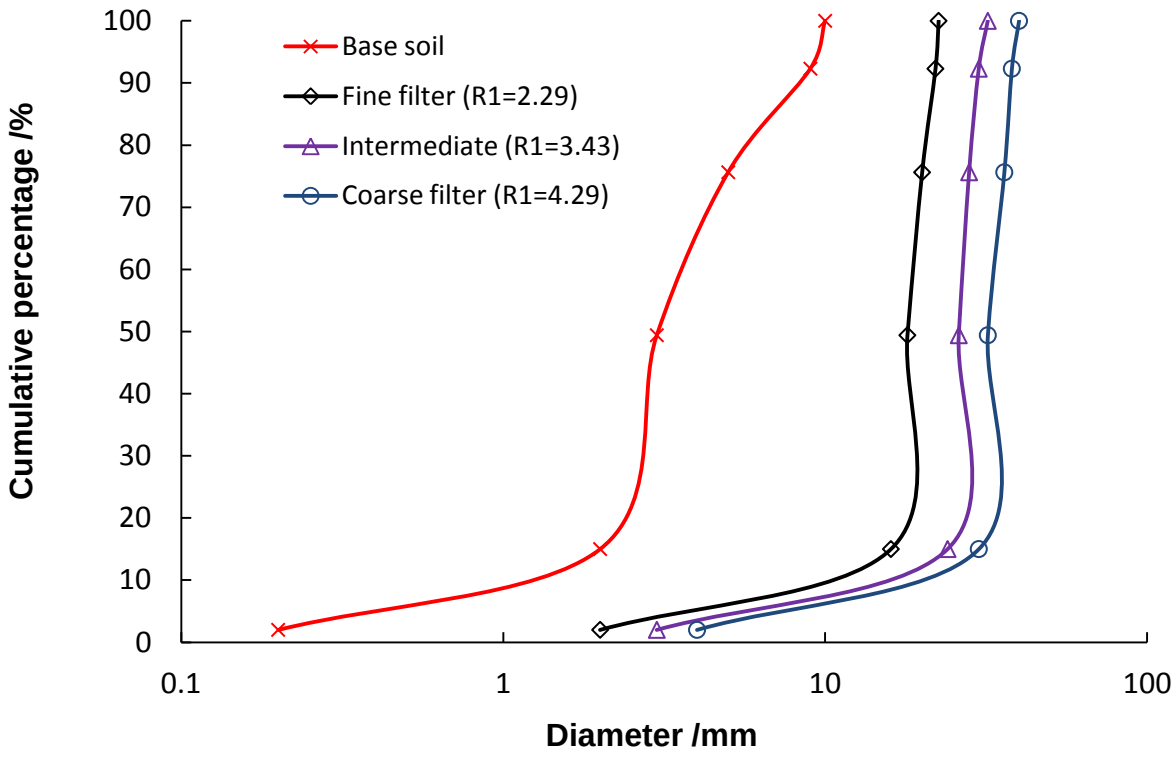
Cumulative percentage /%
100
90
80
70
60
50
40
30
20
10
0
0.1
1
10
100
Diameter /mm
Base soil
Fine filter (R1=2.29)
Intermediate (R1=3.43)
Coarse filter (R1=4.29)

Figure 6
Click here to download high resolution image

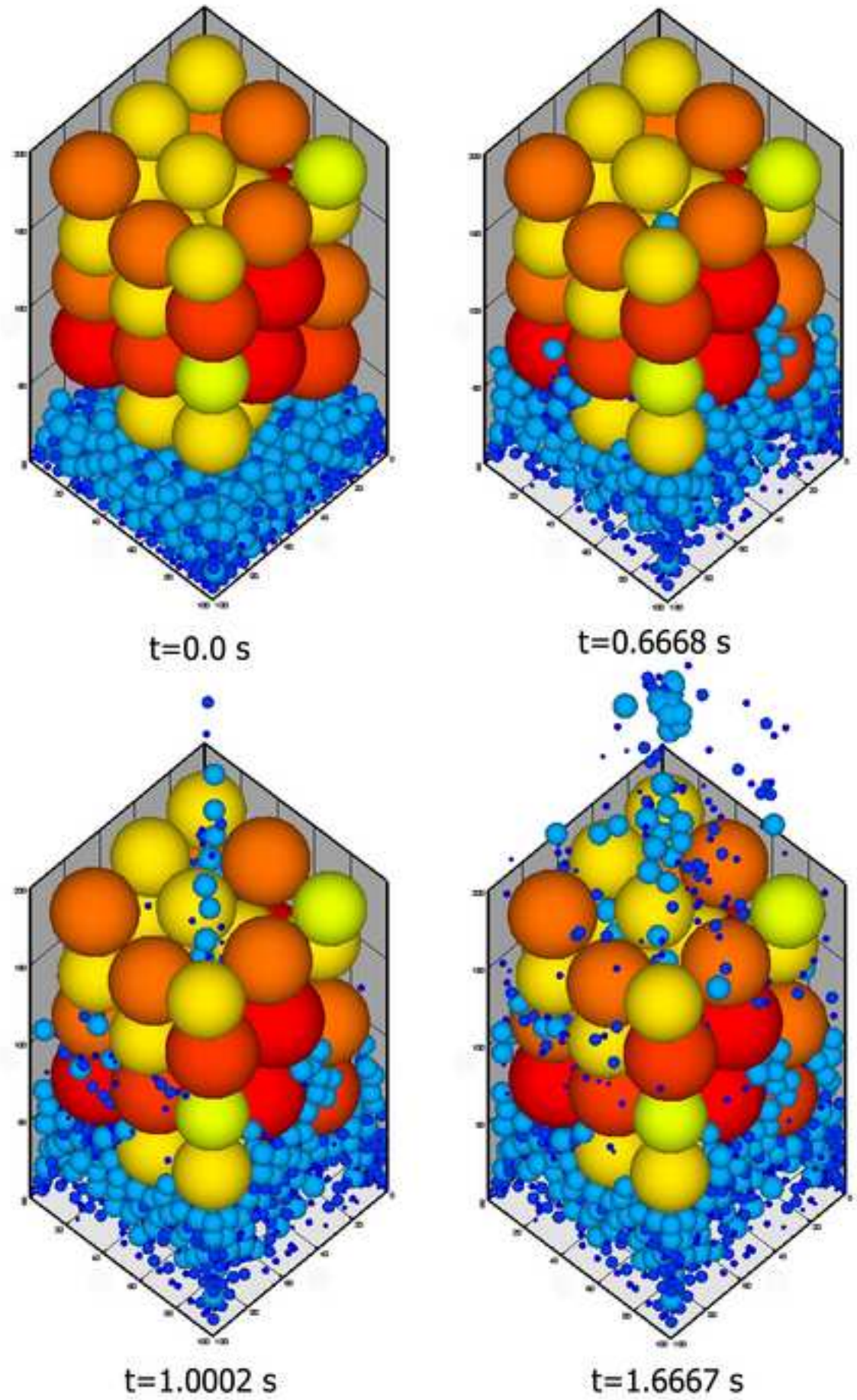

Figure 7

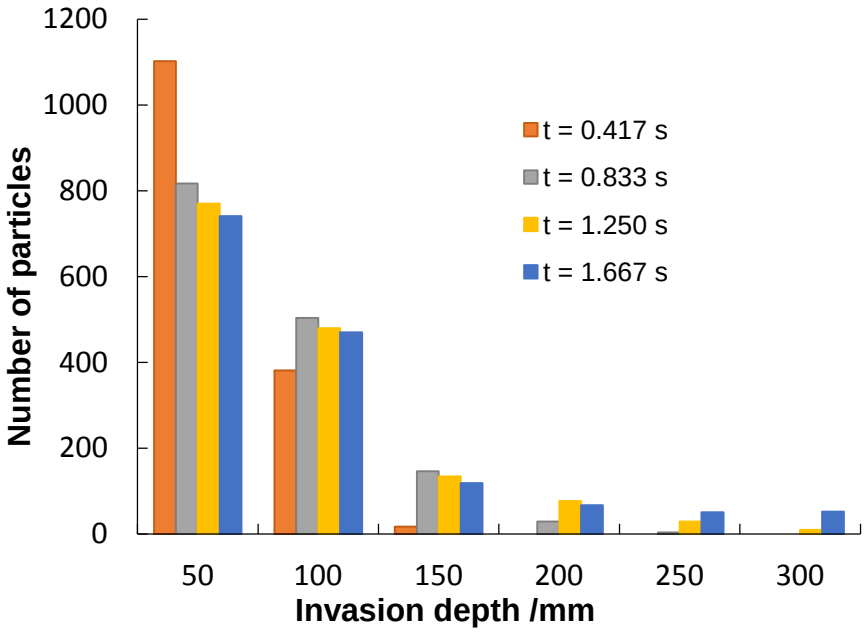
1200
1000
800
600
400
200
0
Number of particles
50
100
150
200
250
300
Invasion depth /mm
t = 0.417 s
t = 0.833 s
t = 1.250 s
t = 1.667 s

Figure 8
Click here to download high resolution image

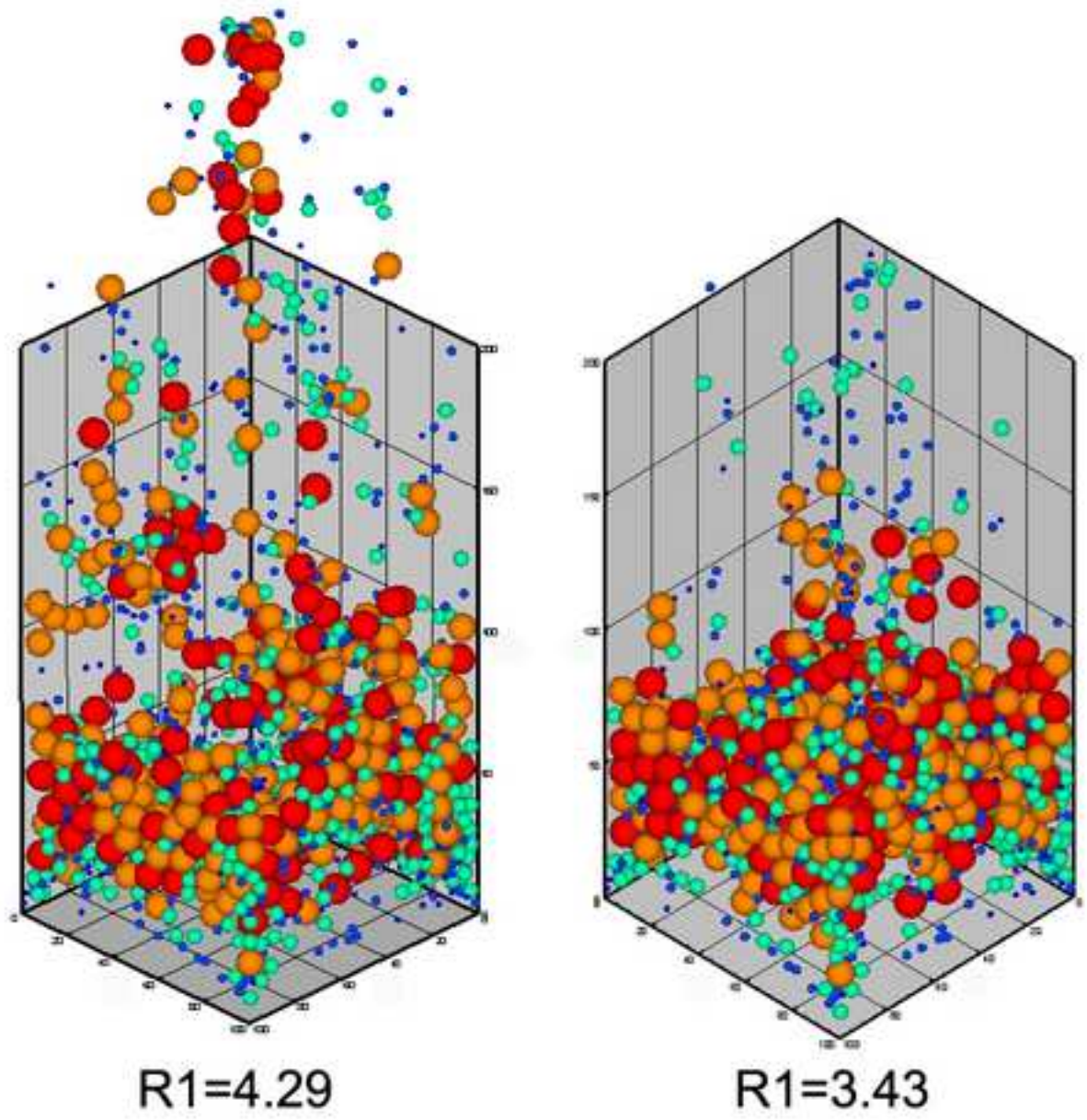

Figure 9

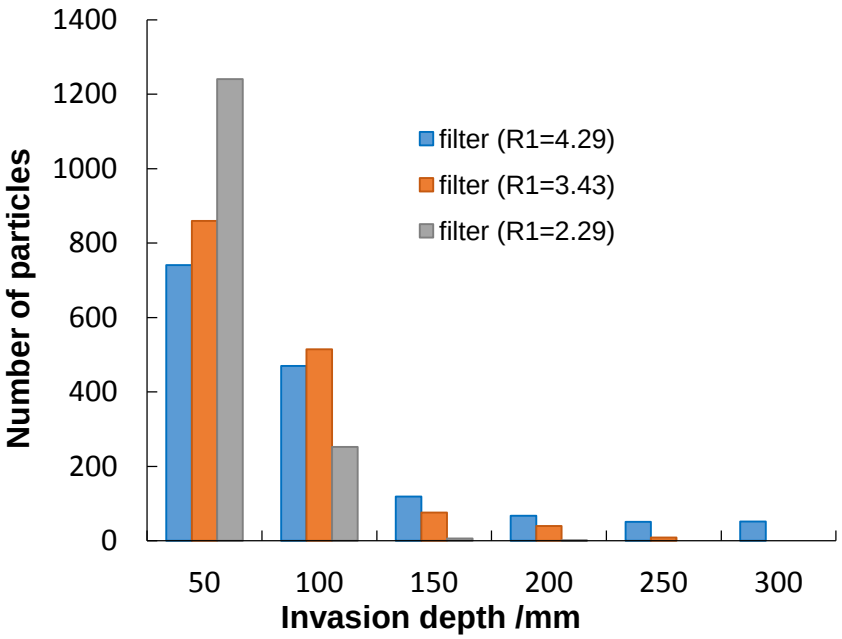
1400
1200
1000
800
600
400
200
0
Number of particles
filter (R1=4.29)
filter (R1=3.43)
filter (R1=2.29)
50
100
150
200
250
300
Invasion depth /mm

Figure 10

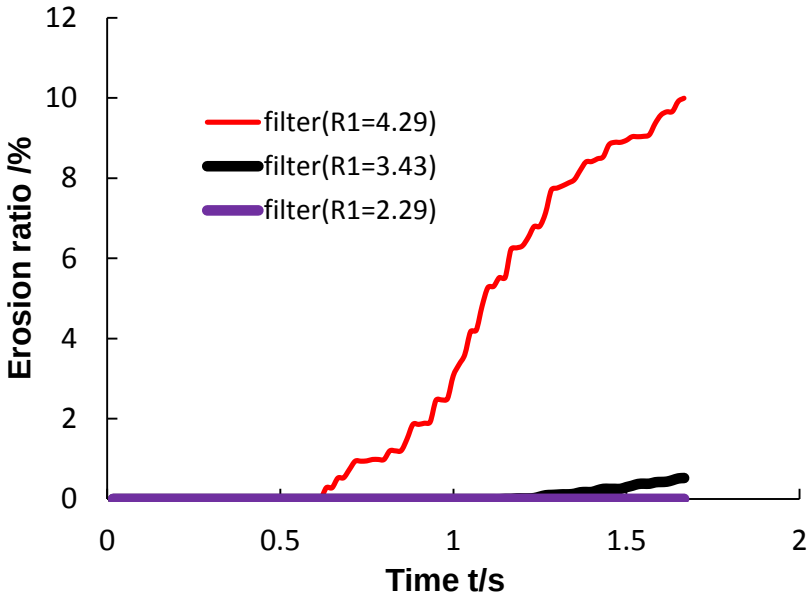
12
10
8
6
4
2
0
Erosion ratio /%
filter(R1=4.29)
filter(R1=3.43)
filter(R1=2.29)
0
0.5
1
1.5
2
Time t/s

Figure 11
Click here to download high resolution image

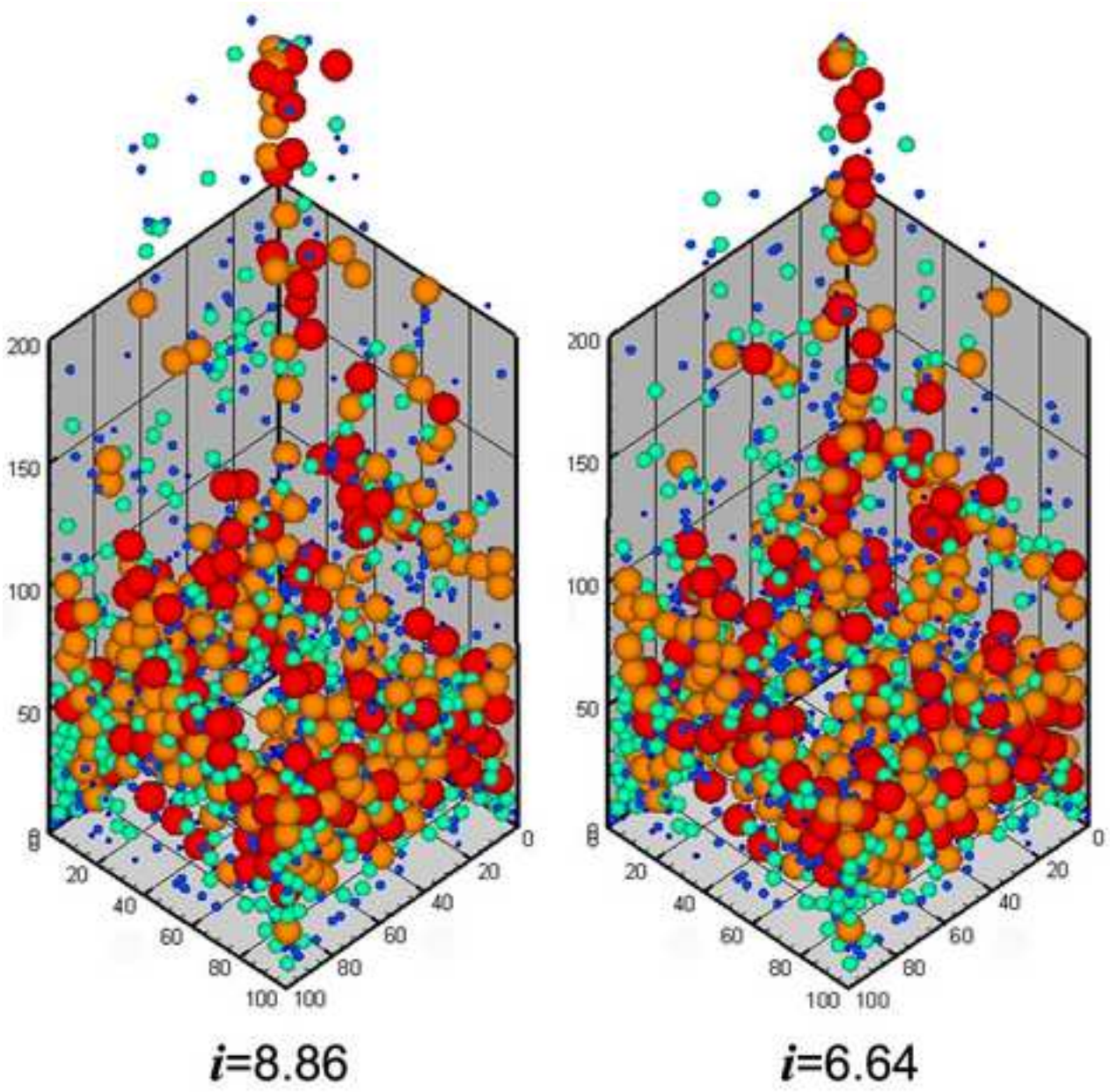

Figure 12

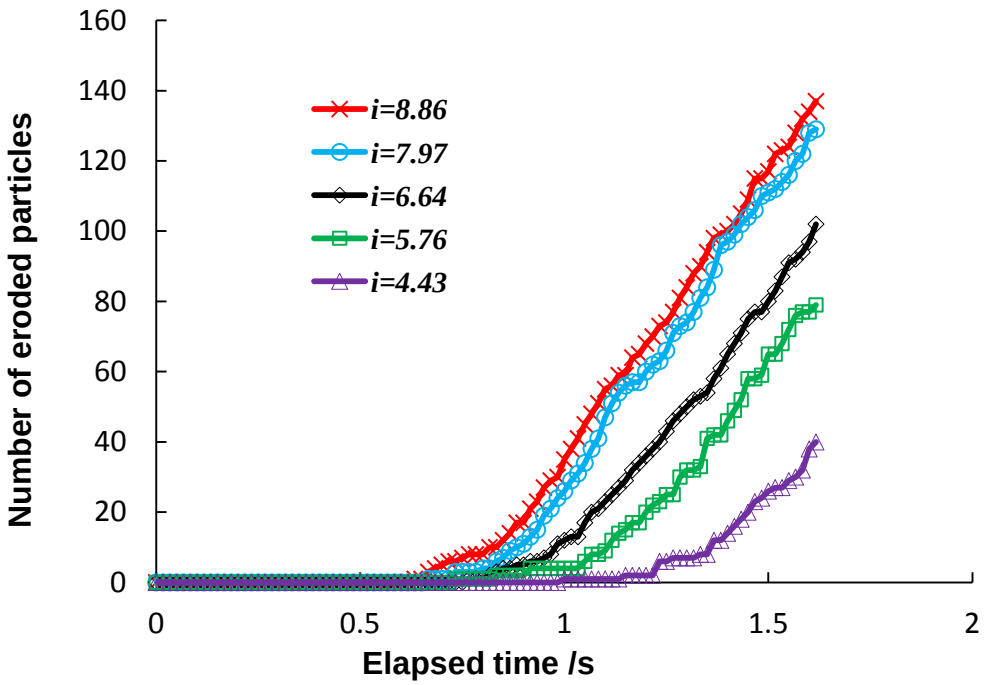
Number of eroded particles
160
140
120
100
80
60
40
20
0
0
0.5
1
1.5
2
Elapsed time /s
i=8.86
i=7.97
i=6.64
i=5.76
i=4.43

Figure 13

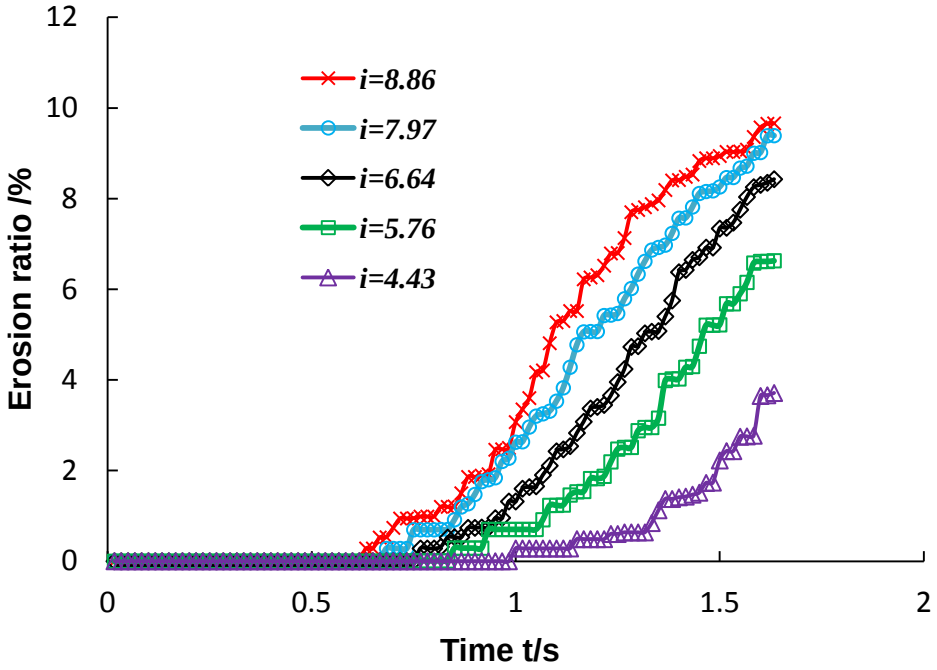
12
10
8
6
4
2
0
Erosion ratio /%
0
0.5
1
1.5
2
Time t/s
i=8.86
i=7.97
i=6.64
i=5.76
i=4.43